A Three-dimensional Numerical Model of a Critical Flow in a Collapsed Tube

Marc Thiriet

INRIA

INSTITUT NATIONAL DE RECHERCHE EN INFORMATIQUE ET EN AUTOMATIQUE

A Three-dimensional Numerical Model of a Critical Flow in a Collapsed Tube

Marc Thiriet

No 3867

2000

THME 4

ISSN 0249-6399 ISRN INRIA/RR--3867--FR+ENG

INRIA
ROCQUENCOURT

A Three-dimensional Numerical Model of a Critical Flow in a Collapsed Tube

Marc Thiriet*

Thème 4 — Simulation et optimisation
de systèmes complexes
Projet M3N

Rapport de recherche n° 3867 — 2000 — 40 pages

Abstract: The laminar steady flow is computed in a rigid pipe with wall configuration corresponding to a highly collapsed flexible tube conveying a critical flow (Reynolds number of 1210) to investigate the three-dimensional flow characteristics, especially in the distal segment. The tube shape, in both axial and transverse planes, is designed from ultra-sound measurements performed on the actual Starling resistor. The opposite walls in the distal tube segment come into contact; the tube then diverges to reach a circular uniform exit segment. The Navier-Stokes equations, associated to the classical boundary conditions, were solved by a finite element method (P1 - P1 bubble element). Where the opposite walls are into contact, the fluid flows through two small drop-shaped outer passages. In the downstream divergent, in- and up(bottom)ward jets are associated to flow separations and to flow characteristics behind an immersed stationary body.

Key-words: Collapsed tube flow, Contact, Finite element method.

* Email: Marc.Thiriet@inria.fr

Unit de recherche INRIA Rocquencourt
Domaine de Voluceau, Rocquencourt, BP 105, 78153 Le Chesnay Cedex (France)
Tlphone : +33 1 39 63 55 11 - Tlcopie : +33 1 39 63 53 30

Modèle numérique de l'écoulement critique dans un tube collabé

Résumé : L'écoulement laminaire permanent est étudié numériquement dans un tube rigide dont la forme est définie par celle d'un tube compliant fortement collabé dans des conditions critiques du système fluide-conduit (nombre de Reynolds calculé à partir du diamètre en entrée et de la vitesse débitante de 1210). Il s'agit de préciser les caractéristiques de l'écoulement tridimensionel, en particulier dans le tronçon en aval du tube collabé. Les configurations axiale et transversale du vaisseau sont dictées par les mesures ultra-sonores effectuées sur un tube en élastomère confiné. Les parois opposées du tube dans son tronçon en aval sont en contact sur une longueur d'environ 1.2 % de la longueur totale du tube, du point de contact à une ligne de contact. Un divergent/convergent en aval est imposé par la fixation à un tuyau rigide. Les équations de conservation de la masse et de la quantité de mouvement sont résolues par la méthode des éléments finis dans le cas du fluide newtonien incompressible, avec des conditions aux limites classiques (élément P1 bulle - P1). Le fluide s'écoule par les deux petits canaux latéraux dans la zone de contact. Dans le divergent/convergent en aval, un jet provenant de chacun de ces canaux se dirige vers l'intérieur et le haut (bas) de la lumière du tube. Des décollements et un comportement du fluide du type de celui observé en arrière d'un corps rigide immobile immergé y sont associés.

Mots-clés : Contact, Eléments finis, Equations de Navier-Stokes, Tuyaux collabables.

1 Introduction

1.1 The context

Endoscopic examinations of leg superficial veins show that these vessels, initially elliptical, can collapse. The vein is one of the physiological vessels which is modeled by the so-called **collapsible tube**, *i.e.* a compliant pipe able to collapse when subjected to negative transmural pressures p[1](appendix A).

The dynamics of collapsible conduits depend upon the coupling between the fluid and the flexible wall *via* the non-linear relationship, the so-called **tube law**, which relates the transmural pressure p to the cross-sectional luminal area A_i. The p *vs.* A_i relationship exhibits a sigmoidal shape. The collapsing process is, indeed, characterized by large variations in A_i associated with small variations of p when p is slightly negative. The theoretical tube law is obtained on an infinitely long straight tube, with a set of assumptions (appendix B).

Because the unstressed (subscript 0)[2] cross-sectional shape is elliptical, the tube collapses with a two-fold symmetry[3]. During the collapse of a flexible duct, with elliptical neutral cross section, three characteristic transmural pressures may be defined : (i) the **ovalisation pressure** p_o, for which the radius of curvature at the wall point of minimal curvature becomes infinite, (ii) the **contact pressure** p_c (point-contact pressure), at which the opposite sides touch, and (iii) the **osculation pressure** p_ℓ (or line-contact pressure), when the radius of curvature at the contact point becomes infinite. Four distinct pressure ranges are bounded by these characteristic transmural pressures: (i)

[1]Compliant vessels undergo deformations under varying transmural pressures p, defined as the difference between the internal and the external pressures $p = p_i - p_e$.

[2]The stress-free state is here defined by $p = 0$.

[3]A greater number of lobes can be observed in tubes of unstressed circular cross section. When the unstressed cross section is circular and $p < 0$, the compliant tube keeps a circular cross section down to the **buckling pressure** p_b. From this mechanical state, a small decrease in transmural pressure p produces a large change in cross-sectional shape and area A_i. Different modes of collapse can be observed according to the number N of lobes, *i.e.* the open part of the collapsed tube lumen. The lobe number depends both on the tube properties (geometry and rheology) and on the boundary conditions.

$p_o \leq p \leq 0$, especially when the tube ellipticity k_0 is close to unity (*i.e.* the cross-sectional shape is close to the circle), (ii) $p_c \leq p \leq p_o$, an interval characterized by a high tube compliance, (iii) $p_l \leq p \leq p_c$, during which the curvature at the contact point decreases, and (iv) $p \leq p_l$ during which the contact line expands laterally.

In the slightly negative range of transmural pressures, both the decrease in tube cross-sectional area and high compliance entail a low wave speed (appendix C). The **Mach number** is one of the main governing parameters of the collapsible tube flow. Critical conditions are associated with the concept of **flow limitation**: downstream pressure informations travelling with the wave speed c cannot migrate upstream from the critical section, where the cross-sectional average fluid velocity U is equal to c [1].

Works on physiological problems are based on modelling. Experiments and numerical tests are carried out on the so-called **Starling resistor**. The test section is composed of a thin-walled compliant straight pipe, of a given length L, mounted on rigid tubings at its ends and enclosed in a rigid transparent chamber, where the pressure p_e can be adjusted. Both the inlet p_{i1} and the outlet p_{i2} internal pressures are measured. In its collapsed configuration, the tube exhibits a throat near the exit, where the opposite walls are the nearest and can come into contact (Fig. 1). As soon as the opposite walls come into contact, the flow splits into two separate streams: the fluid flows through two small tear-drop-shaped outer passages in the contact segment (while the lumen height decreases, the length between the tube axis and the edge increases in association with a variation in the wetted tube perimeter as soon as a contact line is set). Downstream from the throat, end effects give birth to a reopening segment. In this segment, the flow must be characterized by jets and flow separations.

The one- and two-dimensional studies of collapsible tube flow has been developed by different research groups (for brief reviews, *e.g.* [2][3][4]). Model studies raise questions which, although they do not have necessarily physiological implications, have their own physical interests, like self-excited oscillations. A lot of models enlighten on flow separation downstream the col-

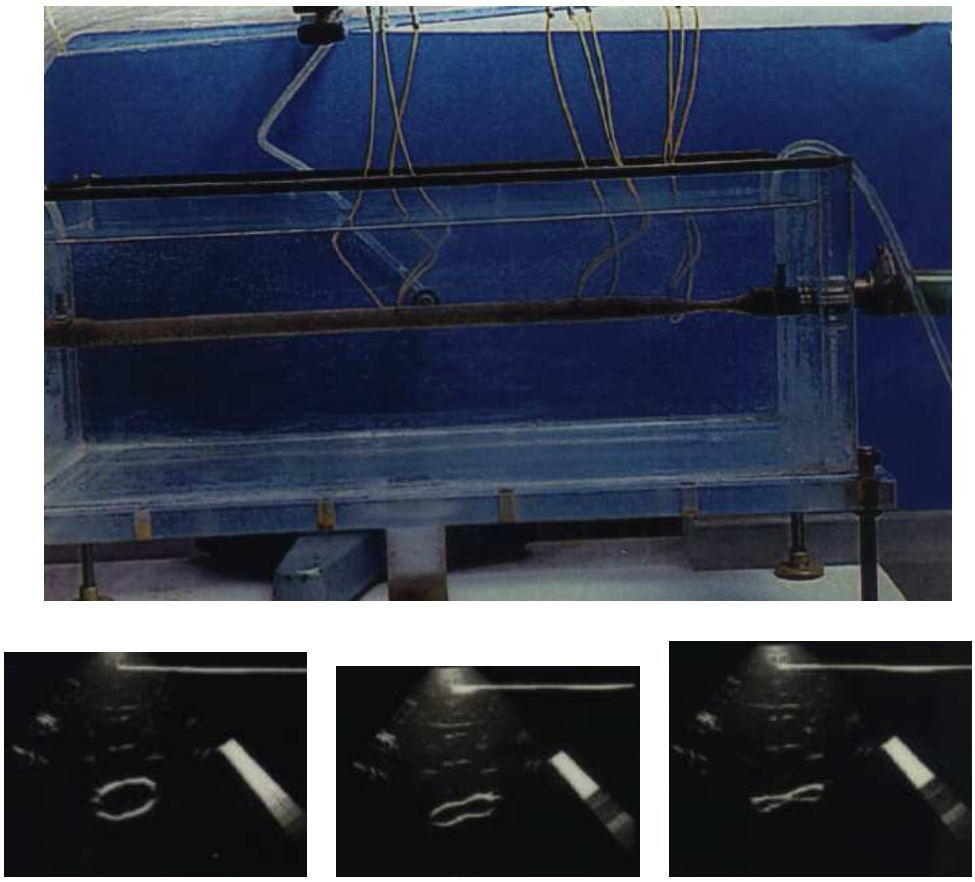

Figure 1: Top: experimental set-up composed of a steady collapsed tube in a perspex chamber, with a contact zone near its exit upstream from the divergent induced by the tube attachment. Bottom: ultra-sound measurements of cross-sectional areas at three different stations along the collapsed tube made by C. Ribreau.

lapsed tube throat. However, detailed analyses of the tube-fluid mechanics need three-dimensional studies both in fluid mechanics and in solid mechanics. Time-dependent velocity profiles measured by laser Doppler velocimetry in an oscillating collapsible tube, in the plane formed by the tube axis and the collapse short axis [5] and measurements in a rigid laterally-enlarged constriction [6] confirm the need to explore three-dimensional flows. At the present time, three-dimensional models, over-simple in fluid mechanics but more complex in solid mechanics, without incorporating contact, are developed [7]. Besides, flow effects on endothelial cell cultures are studied in perspex tube, the configuration of which mimic those of collapsed tube [8].

The present work is aimed at understanding the three-dimensional velocity field in steady flow through a flexible tube which is highly collapsed at its downstream end, because the upstream and downstream effects of the stream division on the flow field are still ignored. In a first approach, owing to the complex nature of the fluid-wall interaction, the laminar steady velocity field was computed in a rigid pipe with wall configuration corresponding to a flexible tube conveying a critical flow. The critical reference state is defined by a localized throat near the tube outlet, where the fluid speed may become twenty times the cross-sectional average velocity.

2 Method

Collapsed-tube model design The tube shape, in both axial and transverse planes, was designed from ultra-sound echographic measurements (Edap Sonedap 10) performed in steady conditions on an actual Starling resistor. The thin-walled collapsible tube (unstressed major semi axis a_0 of 7.5 mm, unstressed tube ellipticity k_0 of 1.2, unstressed wall thickness h_0 of 0.3 mm, $h_0/a_0 = 0.04$), attached to rigid pipes (internal diameter of 13.5 mm) was subjected to an initial lengthening of 1.5 %. The wall material was supposed to be incompressible (Poisson ratio ν of 0.5). The elastic modulus was calculated with an indirect method [23]: The measured point-contact pressure $p_c = 90\ Pa$, and the theoretical normalized point-contact pressure for the ge-

ometrically defined compliant tube $\tilde{p}_c = -2.9$; the transmural pressure scale K is then equal to 31 Pa. The wall bending stiffness $E = 6K(1-\nu^2)a_0^3/h_0^3$ is thus equal to $2.2\,10^6$ $N.m^{-2}$.

The steady configuration of interest was defined with the following data (Fig. 2). The critical flow rate was equal to 16.2 $ml.s^{-1}$. The Reynolds number based on inlet tube diameter and cross-sectional average velocity $Re = 1210$. The imaged stations, which are the input cross sections of known size of the geometrical domain, were located at the following axial positions:

$$z = 210,\ 300,\ 320,\ 340,\ 350,\ 356,\ 363,\ 370,\ 377\ mm.$$

The digitized cross-sectional contours are compared to equivalent cross-section geometry derived from a theoretical model of an infinitely long flexible tube submitted to a negative transmural pressure [21]. The coordinates of points of the wetted perimeter are computed from the coordinates of the mid line and the corresponding angle between the local horizontal and tangent, knowing the wall thickness.

The whole tube (length of 604.3 mm) is decomposed into three main segments: (i) a set of two uniform circular entrance pipe in series (length of 83.7 and 23.5 mm radius of 8.54 and 6.75 mm respectively), the second short pipe modeling the rigid attachment, (ii) the collapsed tube (length of 383 mm), which is terminated on (iii) a set of two uniform cylindrical pipes (length of 30.4 and 83.7 mm, radius of 6.75 and 8.54 mm respectively), the first short pipe being the exit attachment.

The collapsed tube is subdivided, in the streamwize direction, into three successive segments : (i) a tapered segment (length of 364.5 mm), (ii) a contact zone (axial distance between the point-contact and the line-contact input cross sections of $\sim$ 7 mm, *i.e.* of 1.16 % of the entire tube length or 1.83 % of the collapsed tube length) and (iii) the reopened segment (length of 11.5 mm), which is attached to a circular uniform exit duct. The contact zone is equivalent to a set of two symmetric outward channels; the edge x coordinate increases and the lumen height decreases while the central contact segment rises in length. The reopened segment is only partially divergent: whereas the top and bottom

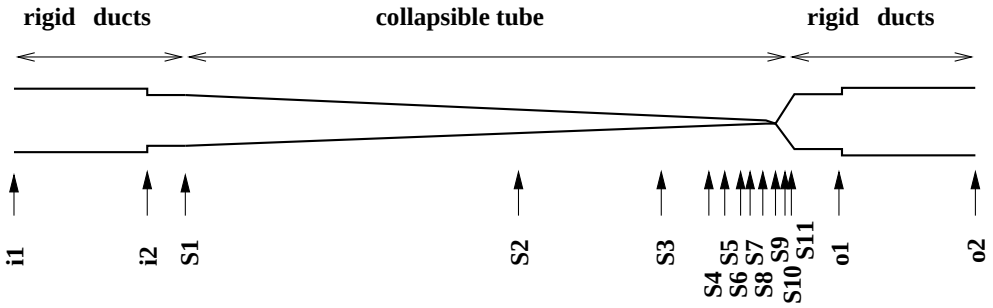

Figure 2: Upper half of the collapsed tube with the measurement sites $\{\mathrm{S}m\}_{m=1}^{11}$ in the one hand and entry (1) and exit (2) cross sections of both the inlet $\{\mathrm{i}m\}_{m=1}^{2}$ and outlet $\{\mathrm{o}m\}_{m=1}^{2}$ rigid ducts.

walls diverge, its edges are convergent.

Fourteen segments are defined in the test section (Tab. 1): (i) two in the set of entrance rigid pipes T1 and T2, (ii) ten in the collapsed tube, T3 to T9 describing the tapered segment, T10 being the contact zone, T11 and T12 defining the reopened segment, and (iii) two in the set of exit rigid conduits T13 and T14. Each segment is bounded in the streamwize direction z by two input cross sections; the generatrices running axially along the tube wall are linearly interpolated lines between corresponding points of the cross-section walls.

Tube mesh Each input cross section quarter is meshed (Fig. 3). The quarter of the wall is defined by the minimal number of nodes (15) to fit the original data (100 points). The segment regions in the planes $x = 0$ (plane normal to the centerplane at the tube axis) and $y = 0$ (centerplane) and the segment wall are meshed using corresponding cross-section nodes. The 5 surfaces are then assembled to give the segment of interest. The 14 segments are merged to provide the whole quarter of the test section surface, the three-dimensional domain of which is then meshed using the software ghs3d (*e.g.* [11]). The

stations	i1	i2	S1	S2	S3	S4	S5	S6
z/d	0	4.9	6.3	18.7	23.8	25.1	26.2	26.8
$\tilde{z} = z/L$	0	0.14	0.18	0.53	0.67	0.71	0.74	0.76
$\tilde{A} = A/A_0$	1	1	1	0.93	0.92	0.88	0.83	0.66
exit section of segment		T1	T2	T3	T4	T5	T6	T7

	S7	S8	S9	S10	S11	o1	o2
	27.1	27.6	28.0	28.4	28.7	30.5	35.4
	0.77	0.78	0.79	0.80	0.81	0.86	1.
	0.52	0.27	0.17	0.72	1	1	1
	T8	T9	T10	T11	T12	T13	T14

Table 1: Geometrical data of the collapsed tube (d: segment T1 diameter). Section i1 is the inlet cross section, i2 a sudden small contraction between the rigid inlet pipes T1 and T2, S1 the upstream attachment cross section, S8 and S9 are contact cross sections, S11 the downstream attachment cross section, o1 a sudden small enlargement between the rigid outlet pipes T13 and T14 and o2 the outlet cross section. The segment set T3 to T9 represents a gradual collapse down to the contact (tapered segment), segment T10 is the contact zone, segments T11 and T12 form the reopened segment.

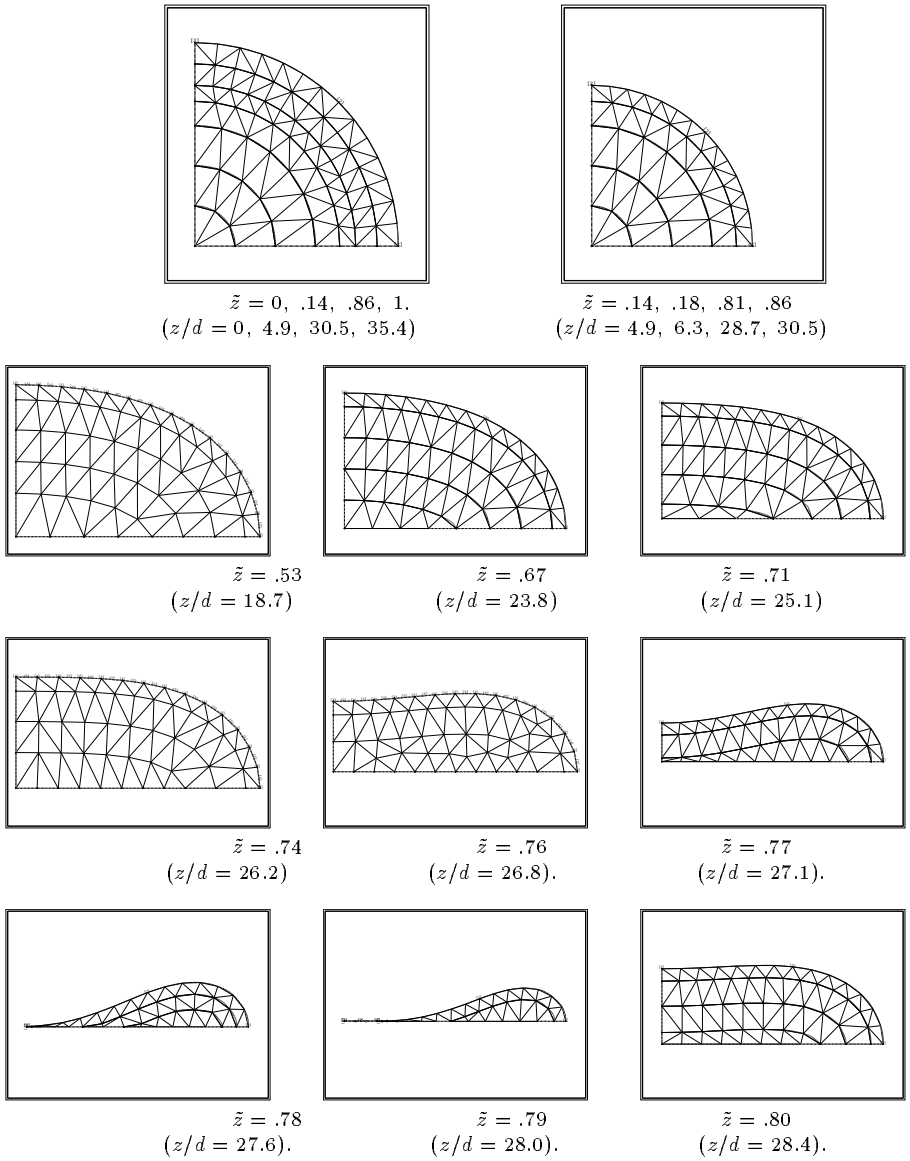

Figure 3: Mesh of the cross section of the collapsed tube through which fluid is flowing steadily. These cross section are measurement stations, in the streamwise direction from top to bottom and left to right, with the corresponding dimensionless axial position $\tilde{z} = z/L$ and the length-diameter ratio z/d ($d = 17,08\ mm$ is the diameter of the cross section of the inlet rigid pipe).

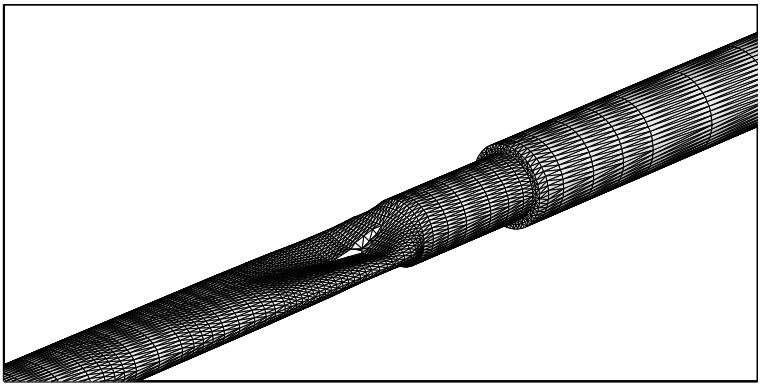

Figure 4: Distal segment of the collapsed tube and the exit rigid ducts in series (right figure side). The tube upper and lower walls diverge while the edges converge down to the rigid attachment downstream the unmeshed contact zone, which is centred along the tube axis.

entire pipe is obtained by symmetry (Fig. 4). The numbers of vertices and of tetrahedra are equal to 15538 and 76484 respectively.

Computational Navier-Stokes model The flow in the collapsed rigid straight tube is governed by the classical equations of fluid dynamics, expressing mass and momemtum conservation in a Cartesian reference frame, when the body forces can be neglected:

$$\rho(\mathbf{u}_{,t} + (\mathbf{u} \cdot \nabla)\mathbf{u}) = -\nabla p + \mu \mathbf{\Delta u} \ , \tag{1}$$

$$\nabla \cdot \mathbf{u} = 0. \tag{2}$$

The momentum equation 1 is computed from its normalized form:

$$St\, \tilde{\mathbf{u}}_{,t} + (\tilde{\mathbf{u}} \,.\, \widetilde{\nabla})\tilde{\mathbf{u}} \ - \frac{1}{Re}\widetilde{\Delta}\tilde{\mathbf{u}} + \widetilde{\nabla}\tilde{p} = 0, \tag{3}$$

where the dimensionless quantities are:

$$\tilde{t} \ = t/T^{\star}, \ \tilde{\mathbf{x}} \ = \mathbf{x}/L^{\star}, \ \tilde{\mathbf{u}} \ = \mathbf{u}/U^{\star}, \ \tilde{p} \ = p/(\rho U^{\star 2}),$$

the superscript * denoting the variable scales, Re and St being the Reynolds and the Strouhal numbers.

The fluid is homogeneous, incompressible and Newtonian, with the water physical properties. For sake of simplicity, the flow is supposed to be steady.

The variational formulation of the set of governing equations (mass and momentum conservation), associated to the classical boundary conditions, were solved by a finite element method designed for unsteady flow. Here, the time was used as an iterative parameter of the solution.

The numerical approximation of the solution of the conservation equations is defined by the variational formulation of the Navier-Stokes equation:

$$\frac{d}{dt}(\mathbf{u},\mathbf{v})+B(\mathbf{u},\mathbf{v})+T(\mathbf{u};\mathbf{u},\mathbf{v})+\ B'(\mathbf{v},p)=<\ l,\mathbf{v}\ >\ ,\ \forall\,\mathbf{v}\in\ V\ \subset\ H^1(\Omega)^3\ , \tag{4}$$

$$B'(\mathbf{u},q)\ =0,\ \forall\ q\in\ \ Q\ \subset\ L^2(\Omega), \tag{5}$$

where $(\mathbf{u},\mathbf{v})$ is the scalar product associated to the space $L^2(\Omega)$, B et B' are bilinear forms ($B(\mathbf{u},\mathbf{v})\ =\ \frac{1}{Re}\Big[(\nabla\times\mathbf{u},\nabla\times\mathbf{v})_{L^2(\Omega)}+(\nabla\cdot\mathbf{u},\nabla\cdot\mathbf{v})_{L^2(\Omega)}\Big]$ for the set of boundary conditions given in [12], $B'\ =\ -\ (\nabla\cdot\ \mathbf{v},p)$), T is a trilinear form ($T(\mathbf{u};\mathbf{u},\mathbf{v})\ =[(\mathbf{u}\cdot\nabla)\mathbf{u}]\cdot\mathbf{v}$), and $<\ l,\mathbf{v}\ >$ the dual product. The functional space V is defined by:

$$V\ :\ \{\mathbf{v}\in\ H^1(\Omega)^3,\ \mathbf{v}|_{\Gamma_1}\ =0,\ \mathbf{v}|_{\Gamma_2}\ =v_{z_{in}},\ (\mathbf{v}\times\hat{\mathbf{n}})|_{\Gamma_3}\ =0,\ p(\Gamma_3)\ =p|_{\Gamma_3}\ \},$$

$\{\Gamma_i\}_1^3$ being a partition of the boundary Γ of the fluid domain Ω : Γ_1 is the wall on which the classical no-slip condition is applied, Γ_2 and Γ_3 are the flow inlet and outlet sections. The inlet boundary condition is a uniform injection velocity. The pressure is set equal to zero at the tube exit ($p|_{\Gamma_3}\ =\ 0$).

The pressure p is defined at the four vertices of the tetrahedron (P_1 element) and the velocity $\mathbf{u}$ at both the vertices and the barycenter (P_1 bubble element). The order of the method is $\mathcal{O}(\xi^2)$ for $\mathbf{u}$ and $\mathcal{O}(\xi)$ for p in the L^2 norm, ξ being the mesh step [13]. The convective term is approximated by the method of

characteristics [14]. The computation is initialized as a potential flow. The solution is obtained via a generalized Uzawa-preconditioned-conjugate gradient method [15].

3 Results

The pressure field is given in Fig. 5. The three-dimensional nature of the flow is demonstrated by few streamlines displayed in Fig. 6. Usual modes of the velocity field representation are used: (i) velocity vector maps in selected planes, (ii) iso-speed contours with a entire scale from zero speed to the maximal velocity of 1.4 $m.s^{-1}$ for an entrance uniform velocity of 0.07 $m.s^{-1}$ in the explored planes, and (iii) streamlines either in planes of interest or in the three-dimensional fluid domain. The flow speed has thus been increased 20 times (critical situation). The investigated planes are (i) the input and interpolated cross sections (planes $z = cst$, cross view), (ii) planes $x = cst$ (side view) and $y = cst$ (top view) in the cartesian reference frame, from the symmetry plane to the wall.

Cross views Scans of the velocity field in a set of cross sections, from the middle part of the collapsed tube to the outlet rigid duct is given in Fig. 7 to 9, with a local velocity scale, given in each figure, to enhance the flow details. The flow is convectively accelerated in its proximal collapsed segment and decelerated in the reopened segment. In the reopened segment, four jets, exiting from the side lobes of the contact zone, head for the top/bottom wall and for the vertical symmetry plane $x = 0$, due to both the divergence of the opposite tube walls and of the convergence of the tube edges. In the reopened segment, the secondary flow is totally different from those observed in symmetrical junctions, characterized by a rapid merge in side jets. In each quarter of cross section, the twinned vortex appears. the outer swirl widen from the top/bottom wall to the lateral wall from station $\tilde{z} = 0.811$ to $\tilde{z} = 0.822$, whereas the tranverse near-axis vortex center gets a back-and forth motion from the symmetry planes.

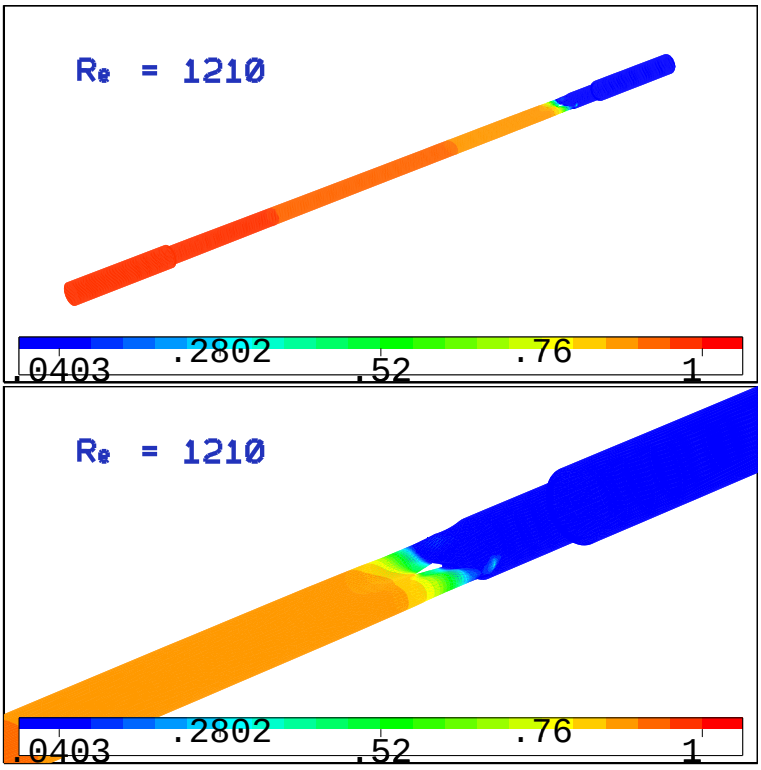

Figure 5: Top: pressure field in the whole tube (duct exit in the right side of the figure, $Re = 1210$). Bottom: zoom on the downstream collapsed tube segment, with the color code of the normalized pressure (p/p_{max}).

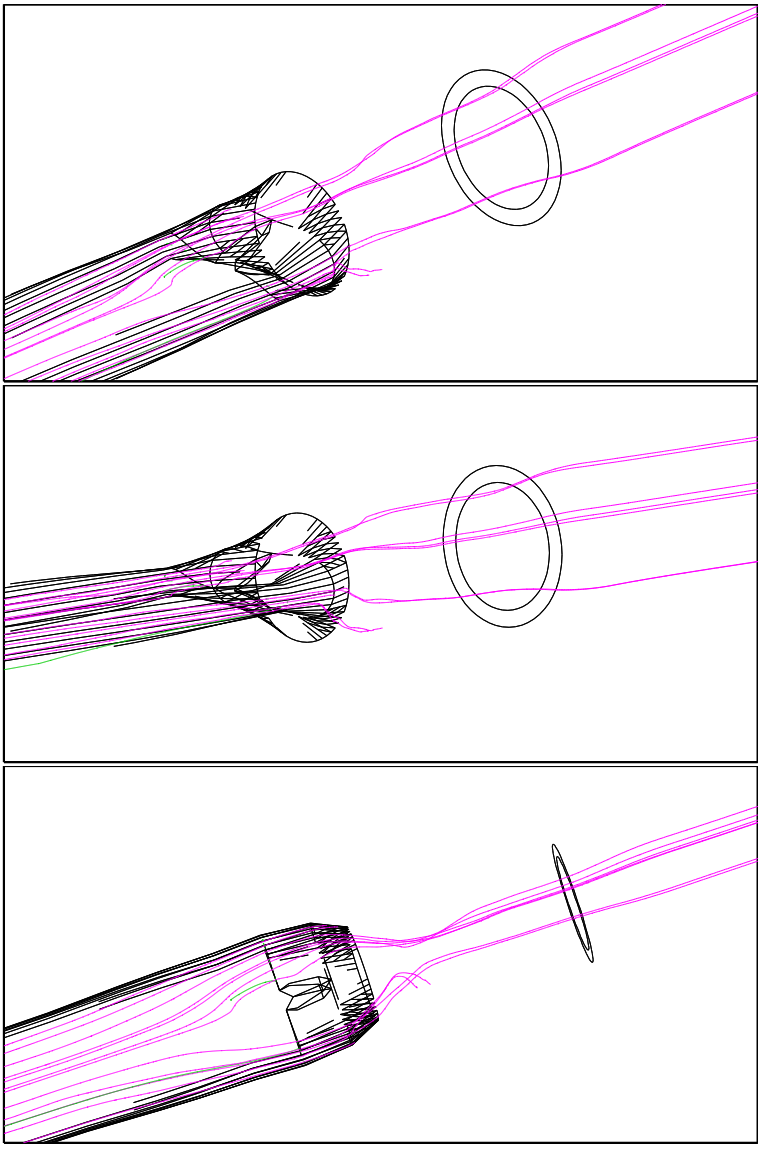

Figure 6: Streamlines in the downstream segment of the collapsed tube and the exit rigid duct. Parts of the tube shape (contact zone, downstream divergent-convergent and the cross section of the rigid exit pipe) are displayed by black lines.

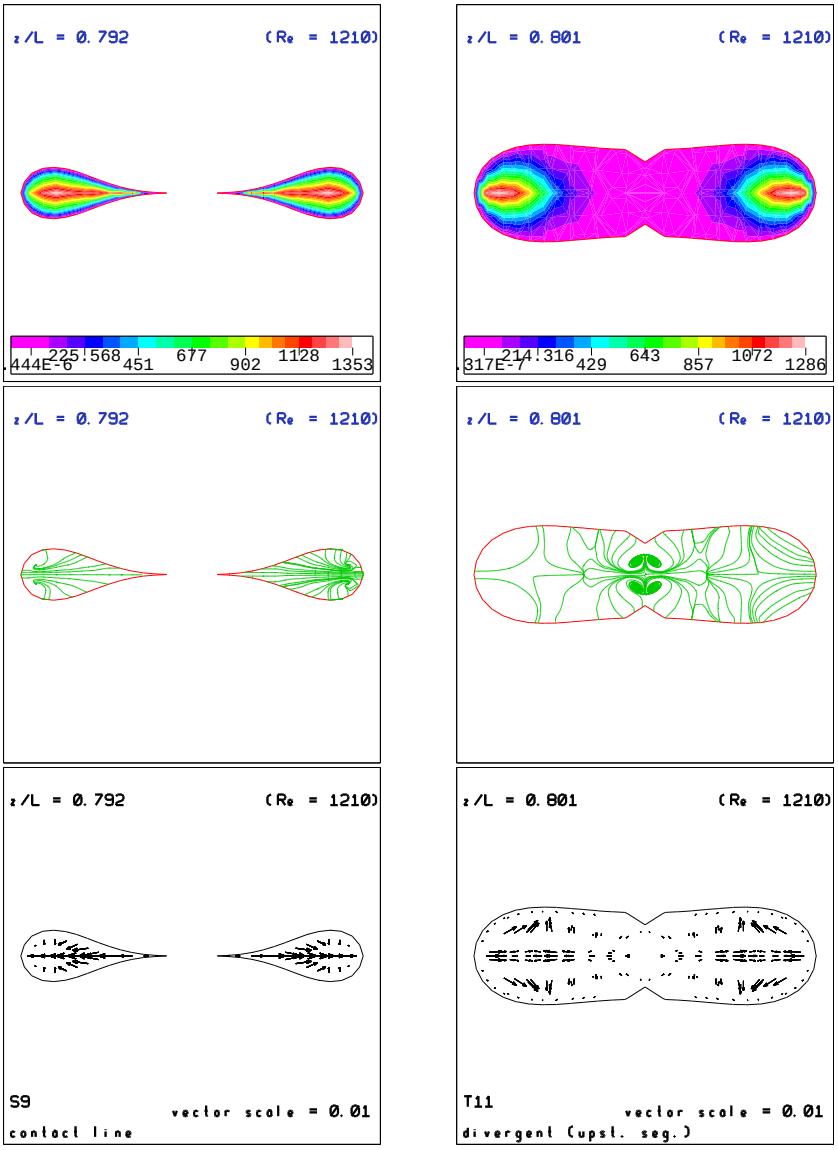

Figure 7: Isospeed contours (top), streamlines (mid), and vector plot (bottom panel) of the transverse component in two cross sections S9 (contact zone) and S10 (upstream segment of the divergent part of the collapsed tube).

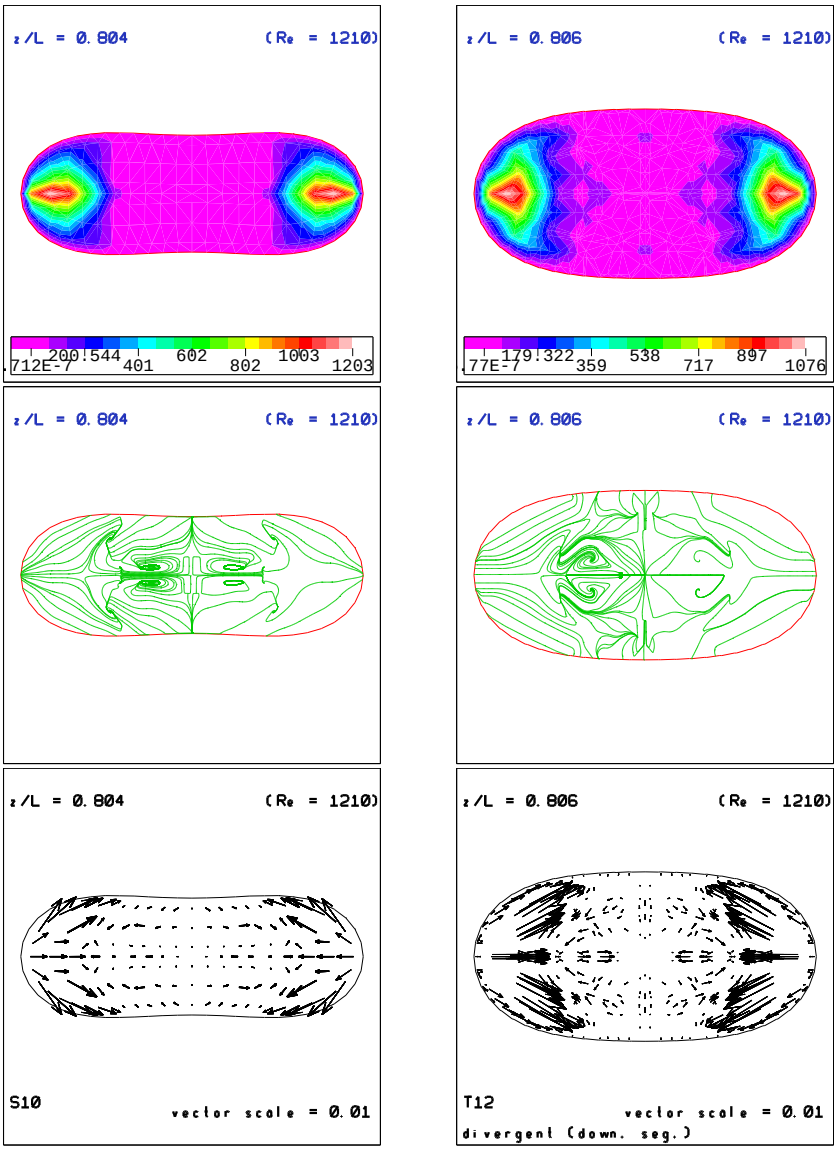

Figure 8: Isospeed contours (top), streamlines (mid), and vector plot (bottom panel) of the transverse component in two cross sections of the distal segment of the collapsed tube.

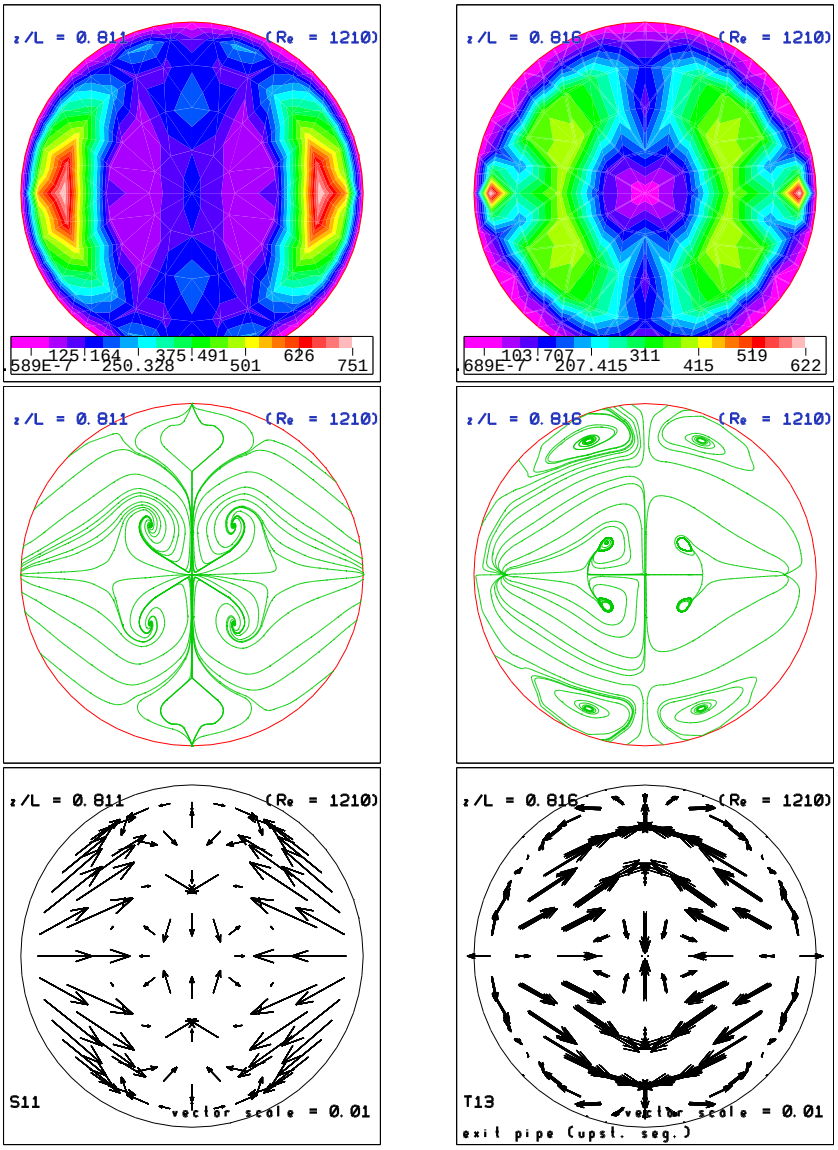

Figure 9: Isospeed contours (top), streamlines (mid), and vector plot (bottom panel) of the transverse component in two cross sections of the exit rigid tube.

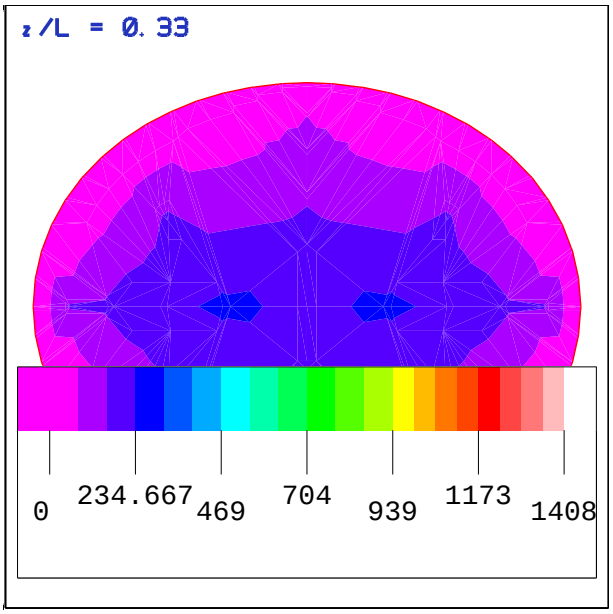

Figure 10: Color code for the full range of the fluid velocity, with isospeed contours in a station located at $\tilde{z} = 0.33$.

The isospeed contours for a set of downstream cross sections are displayed in Fig. 11 to 12 with the same scale, given in Fig. 10 for better comparison.

Side views Scans of the velocity field in a set of planes normal to the centerplane $x = cst$ from the symmetry plane to the tube edge is given in Fig. 13 to 14, with a local velocity scale, given in each figure, to enhance the flow details. Greater part of the side jet is observed in plane close to the tube edge. A saddle point takes place at the single point of contact upstream the reopening of the flexible tube lumen. The flow separation region along the top/bottom wall of the distal segment of the reopened segment cross the vertical symmetry plane and becomes larger near the tube edges. Upstream from it, another flow separation region develops both sides of the vertical mid plane in the proximal segment of the reopened segment. Eddies are located both

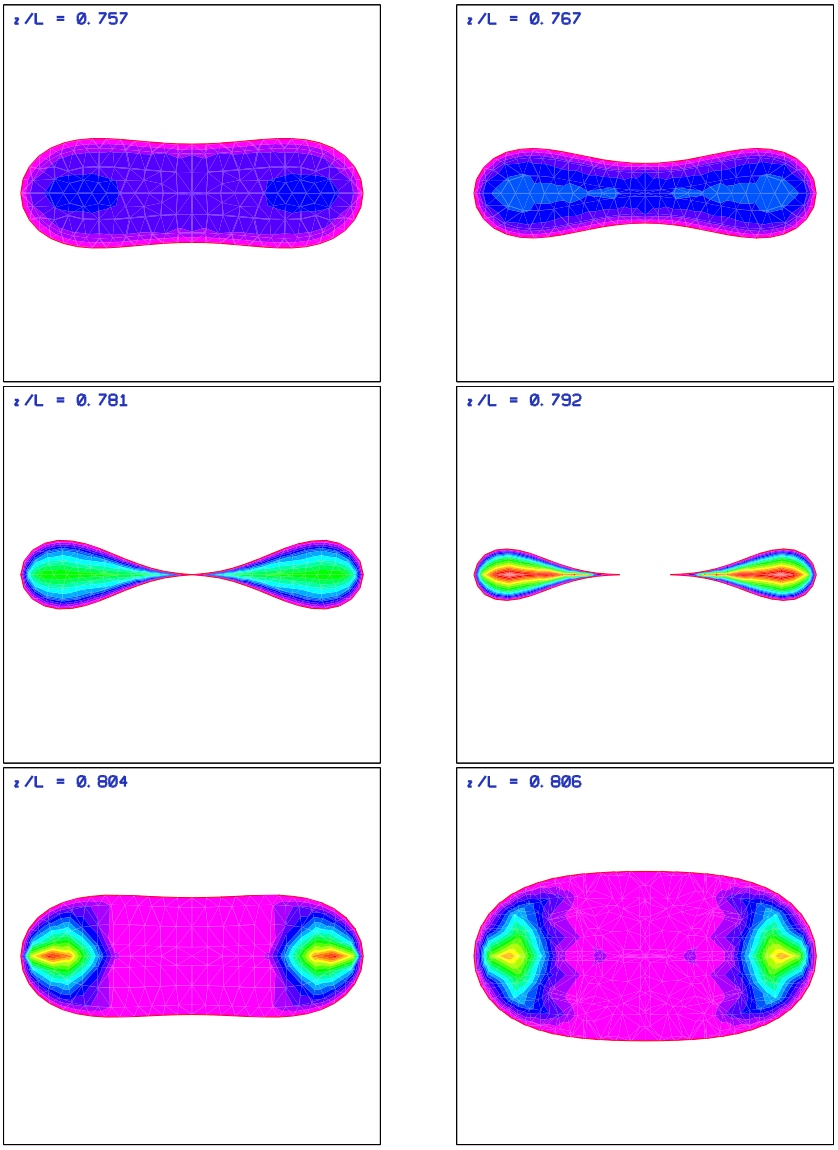

Figure 11: Isospeed contours in a set of cross sections downstream from the contact-point station (the dimensionless axial position is given in the figure).

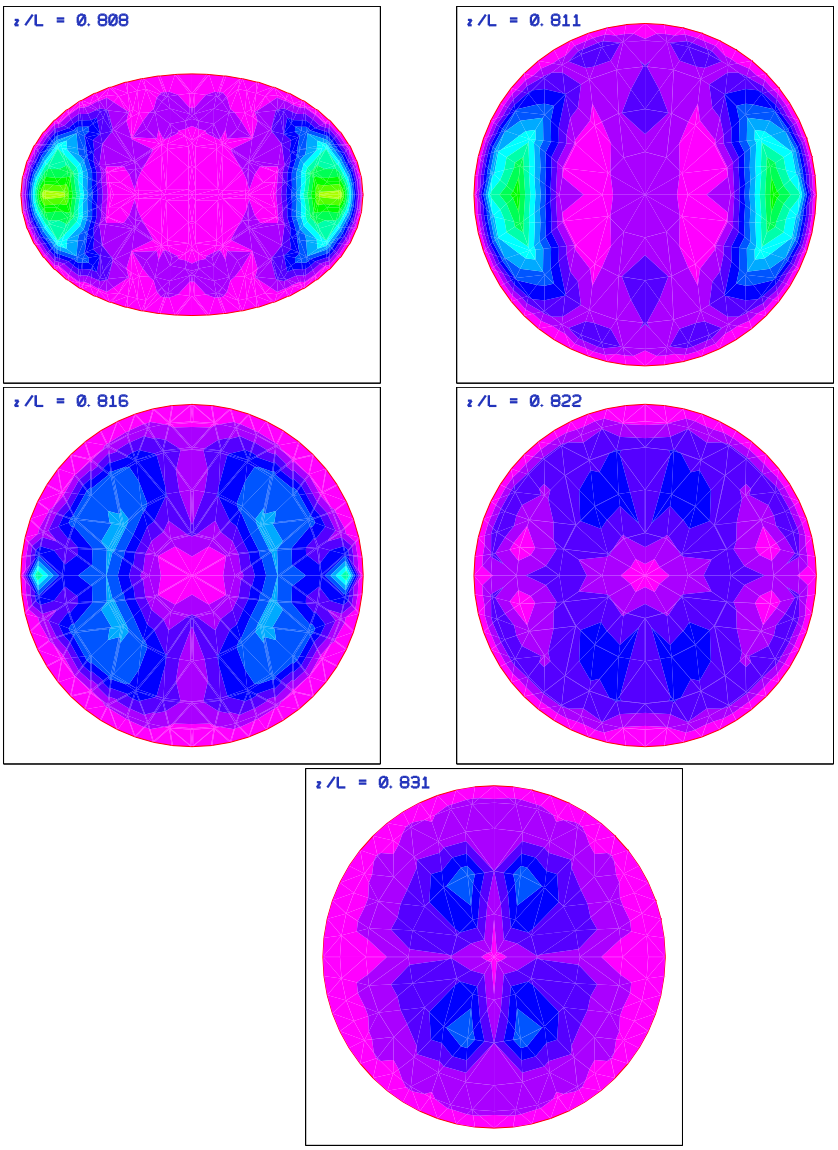

Figure 12: As figure 11 for cross sections nearer the test section outlet.

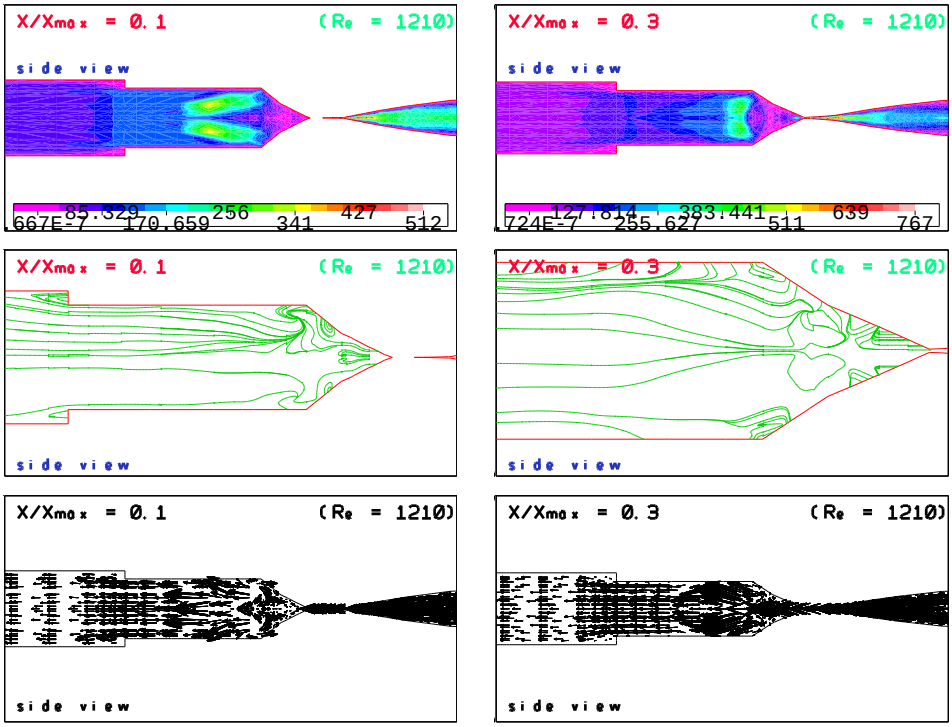

Figure 13: Isospeed contours (top), streamlines (mid), and vector plot (bottom panel) of the in-plane component. Set of sections normal to the centerplane of the collapsed tube and of the exit rigid ducts, downstream from the contact region (duct exit on the left side, $Re = 1210$).

sides of the centerplane and near the top/bottom wall in the entrance region of the rigid outlet duct near the vertical mid plane.

The isospeed contours are displayed in Fig. 15 to 16 with the same scale.

Top views Scans of the velocity field in a set of planes parallel to the centerplane $y = cst$ from the symmetry plane to the tube edge is given in Fig. 17 to 18, with a local velocity scale, given in each figure, to enhance the flow details. The side jets are associated to flow separation region at the edges of the rigid outlet duct, which becomes closer to the compliant tube exit in

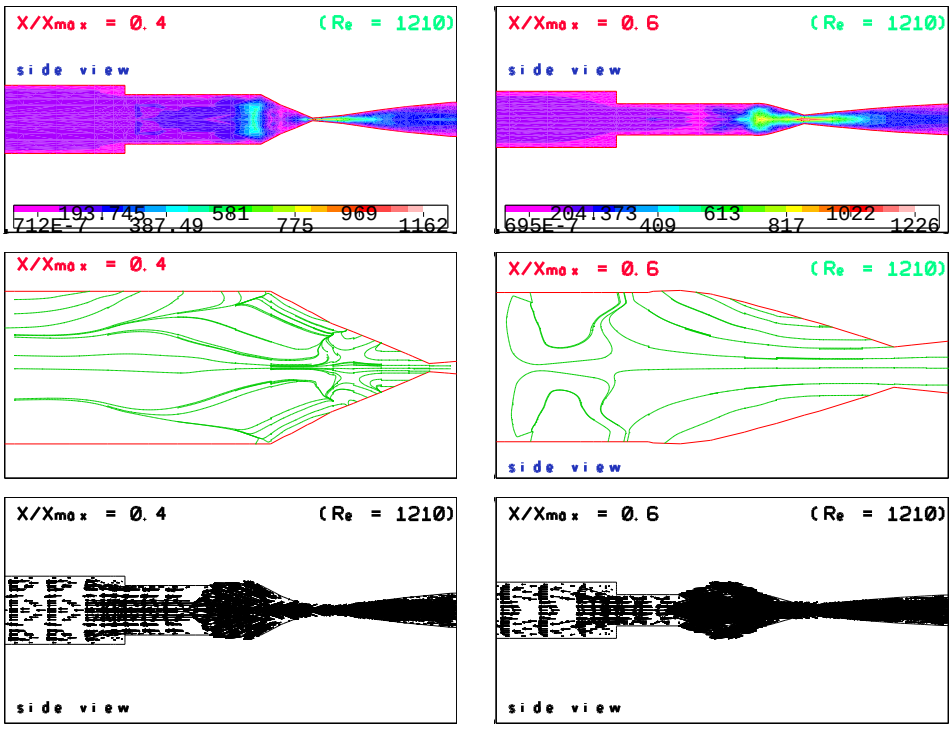

Figure 14: As figure 13 for sections nearer the tube edge.

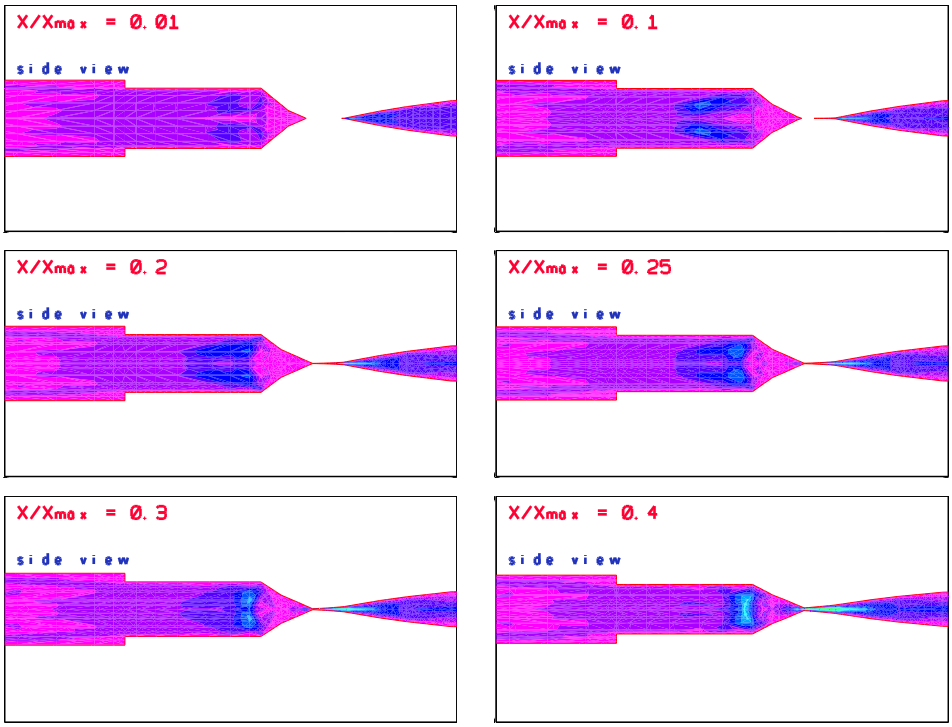

Figure 15: Isospeed contours in the set of sections normal to the centerplane of the collapsed tube and of the exit rigid ducts, downstream from the contact region (duct exit on the left side).

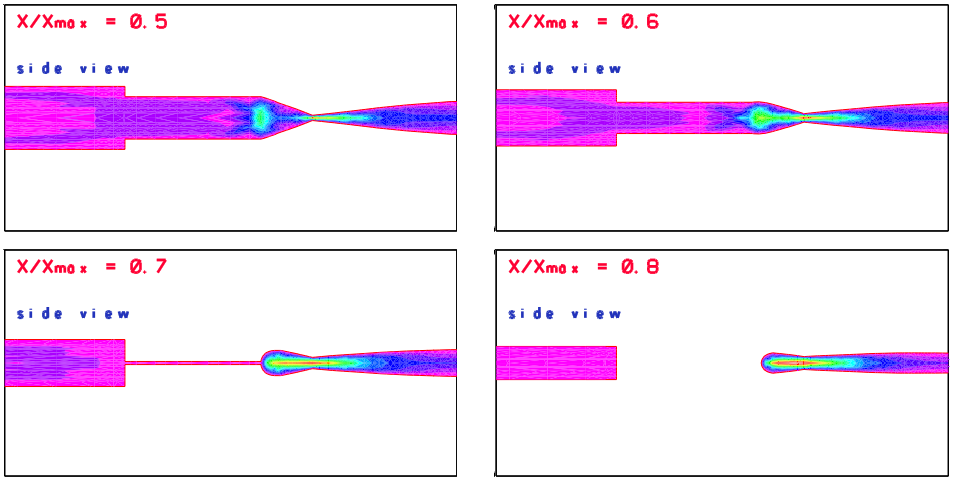

Figure 16: As figure 15 for planes nearer the tube edge.

plane near the top/bottom wall than near the centerplane. In each top/bottom half of the collapsed tube, two swirls occurs behind the contact zone, the center of which is located in the entrance section of the rigid outlet duct.

The isospeed contours are displayed in Fig. 19 to 20 with the same scale.

4 Discussion

4.1 The model

The deformation is not investigated as in Heil work [7] [16], the collapsing process representing a good but complex example of fluid-structure interaction. In a first approach, the wall motion is not investigated and the work is focused on the flow behaviour through a collapsed section with opposite-wall contact and a downstream divergent. The tube wall is then assumed rigid. The tube configuration is designed from the tube shape measured experimentally.

The convergence was supposed to be reached when the L^2 norm of the residuals of the flow quantities are divided at least by a factor of 10^{-6}. It is

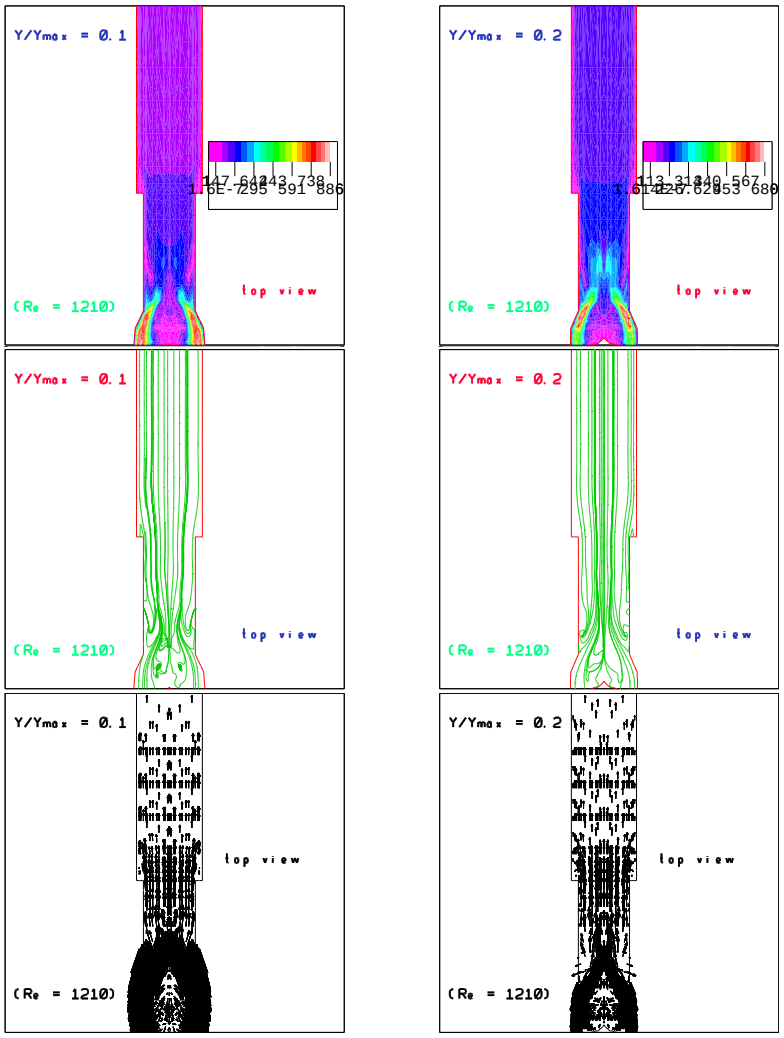

Figure 17: Isospeed contours (top), streamlines (mid), and vector plot (bottom panel) of the in-plane component. Set of sections parallel to the centerplane of the collapsed tube and of the exit rigid ducts, downstream from the contact region (upward streamwize direction).

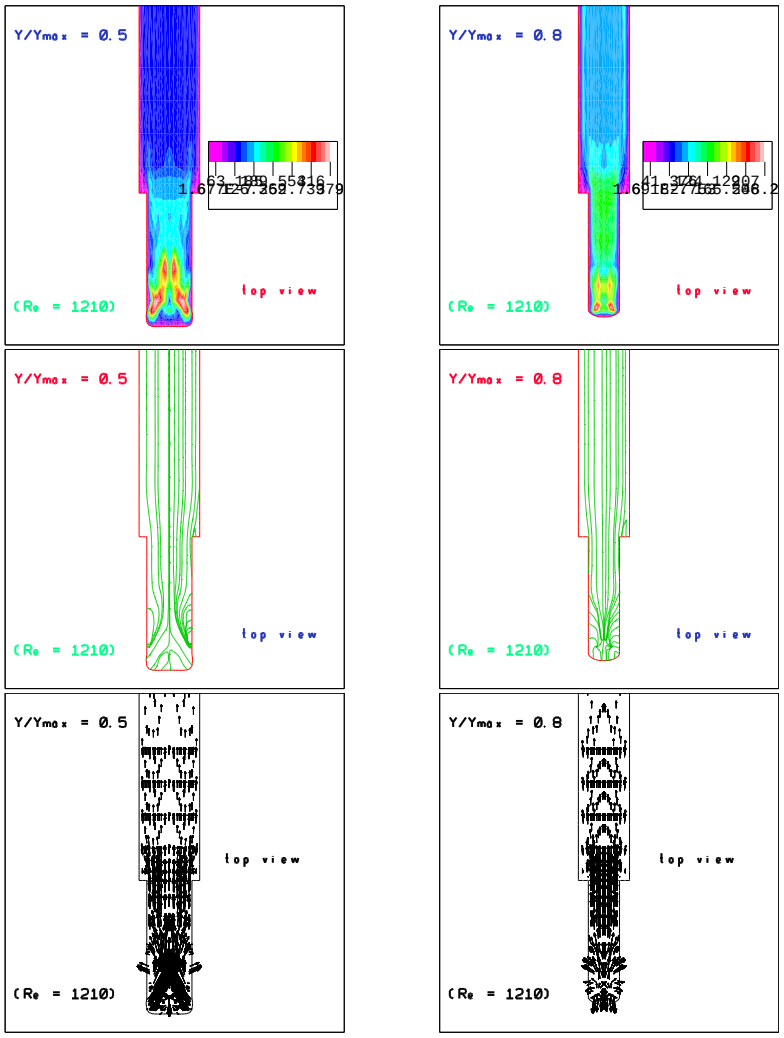

Figure 18: As figure 17 for sections nearer the tube wall.

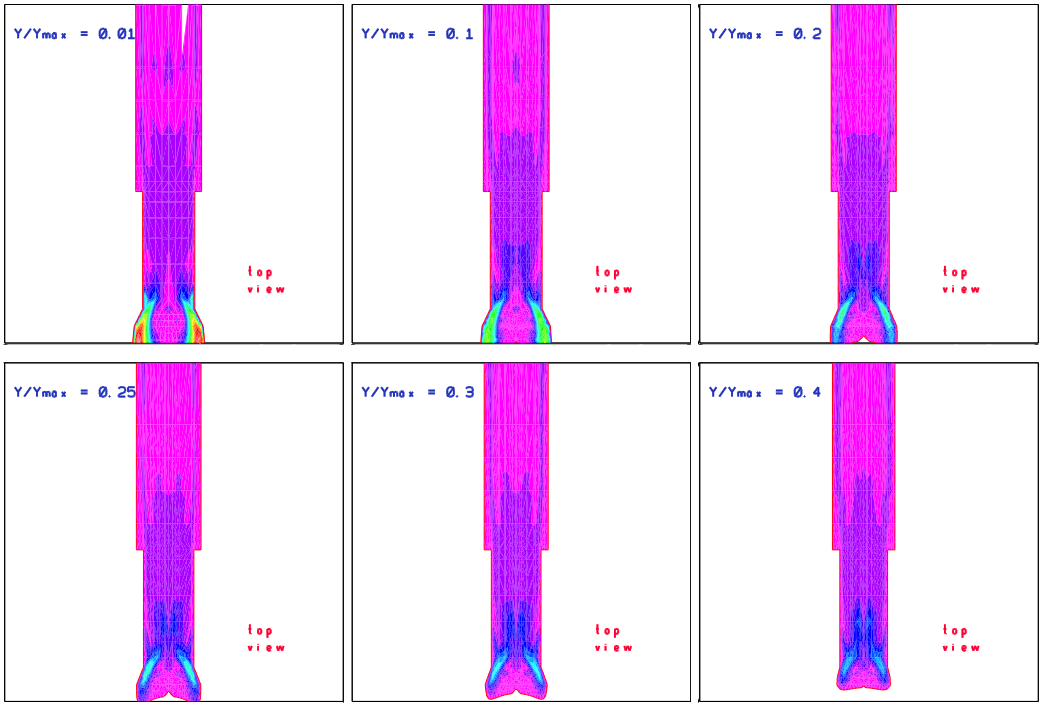

Figure 19: Isospeed contours in the set of sections parallel to the centerplane of the collapsed tube and of the exit rigid ducts, downstream from the contact region (upward streamwize direction).

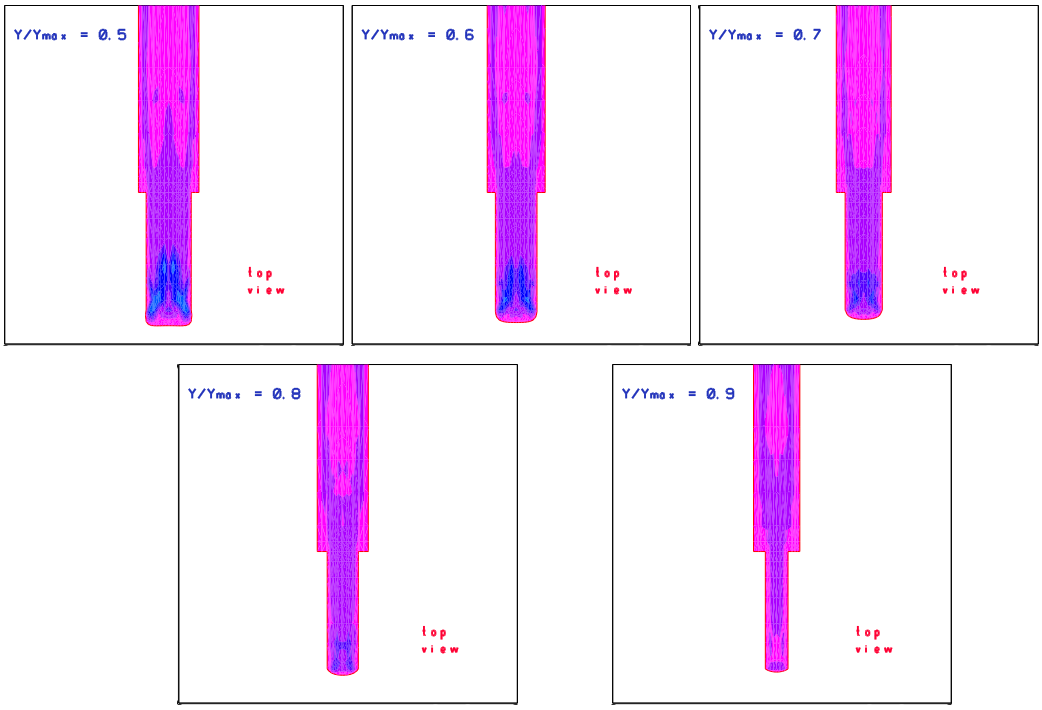

Figure 20: As figure 19 for planes nearer the tube wall.

usually obtained at a time lower than the duration of a characteristic path of four tube length, with the suitable time step.

4.2 Literature data

The laminar steady velocity field is computed in a rigid pipe copied from the flexible tube in critical conditions. Laser-Doppler velocimetry has been performed either in a collapsible tube during self-excited oscillations [5] or in a rigid tube with a throat [6].

The first group of coworkers [5] was the first to measure axial velocity profile (u_z) in thin-walled collapsible tube ($h_0 = 0.15\,mm$, $L_0 = 0.16\,m$). Laminar flow ($Re = 300$) was investigated in the plane normal to the centerplane at the tube axis only, at seven stations (one downstream from the throat). The tube was executing either slow oscillations of more or less small amplitude, during which a back-and-forth fluid motion is set up; the greater the oscillation amplitude, the nearer the tube throat configuration from the opposite wall contact. The authors suggest that the side jets merge downstream the throat because greater variations in fluid velocity occur in the core than near the wall in the investigated plane. However, the flow behaviour can not be precisely described due to the lack both in velocity component measurements and in exploring sites. In the present work, the side jets merge at least partially in the rigid outlet pipe.

The second group of investigators [6] have built a collapsed-like tube, making a pinch in a straight circular perspex tube. The pinch, normal to the centerplane, has a relatively small curvature and is associated to a transverse elargement of gentle curvature (normalized length $\tilde{z} = z/d = \sim 2$, the pinch center is set at $z = 0$). Note that (i) there is no actual opposite wall contact and (ii) the tube configuration is symmetrical both sides of the pinch and does not mimic the collapsed tube. Fully-developed steady laminar flow ($Re = 705$) was explored in planes parallel to the centerplane (two velocity components (u_x, u_z) were measured) in the whole cross section of fifteen stations ($-1 \leq \tilde{z} \leq 3$). The flow is characterized by two strong side-jets, which

remain close to the tube edges downstream from the pinch, with a low-velocity region in the center of the cross section. Immediately behind the pinch center, a reverse flow region is observed. The pinch affects the flow, at least, 2.5 diameter downstream from the pinch center. In our more realistic model, flow separation region appear at both tube edges and the jets are centerwardly directed.

Flow separation was found in a two-dimensional finite element model of a partially deformable channel (one totally rigid wall and a central elastic segment on the opposite wall) conveying a steady laminar flow (Poiseuille entrance condition, $Re = 300$) both at the wall behind the throat and further downstream at the opposite wall [17]. Such geometry does not fit the usual experimental configuration of collapsed tube.

Steady very low Re flow has been studied in a collapsing elastic tube [16]. More or less collapse was observed according to the flow rate Q and external pressure p_e values, without opposite wall contact. The streamlines of the cross flow in the collapsed segment upstream from the throat (see station $z/R_0 = 6.5$ (R_0: unstressed tube radius) in their Fig.6) are similar to those in our model (see station $\tilde{z} = 0.757$). Because no opposite wall contact occurs, the iso-axial-speed contours are closer to the tube axis than in our model. In the throat region and downstream from it, the transverse currents are different, inertial effects and the tube geometry being different.

5 Conclusion

The contact between the opposite walls of a flexible pipe affects greatly the flow. The present study show that the three-dimensional flow structure in steady conditions is defined by a combination of immersed body-like effects and divergent flow. Two side jets emerging from the contact zone of the collapsed tube run centrally and partially merge in the proximal segment of the rigid attachment duct. Between the side jets and immediateley behind the contact zone swirling motions occur. A lateral high velocity stream is still present far

	anatomical vessel	floppy model
tube geometry	curved axis small L/d (bends, junctions, bifurcations) non-uniform lumen	straight axis long tube uniform lumen
wall geometry	varying thickness	constant thickness ($h/R \ll 1$)
wall structure	composite material	homogeneous
wall rheology	viscoelastic	purely elastic isotropic material
cross loading	non-uniform (various environments)	uniform
resting state	tension (axial and azimuthal)	unstressed

Table 2: The physiological vessel and its collapsible model of both uniform geometry and rheology (L/d: length to diameter ratio, h/R wall thickness to hydraulic radius ratio).

downstream in the circular outlet duct, downstream from the flow separation regions along the attachment pipe.

Appendix

A Collapsible tube model

The physiological vessel is modeled by a flexible pipe using numerous hypotheses; the main assumptions are summarized in Table 2.

The vein junctions, the vessel axis curvature, the axial changes in vessel size and rheology and the composite vessel wall are thus neglected.

The vessel deformation may be investigated either in the positive or the negative transmural pressure range. Arteries dilate while pressure waves migrate. The cross-sectional luminal area A_i is varying whereas p is evolving in a range of positive values. The cross-sectional shape may be affected owing to the non-uniform distribution of p over the entire vessel perimeter and to compression of the neighbouring structures. At the opposite, veins may experience huge changes both in cross-sectional area and shape when they are subjected to negative transmural pressures during natural or functional testing maneuvers, whatever the environment.

B Theoretical tube law

The tube law is computed using the following assumptions:

- the tube is straight and infinitely long,
- both the geometry and the mechanical properties are uniform,
- the flexible pipe is subjected to a uniform transmural pressure, both in longitudinal and azimuthal directions,
- the wall is assumed to be thin, homogeneous and purely elastic; the wall thickness, much less than the lowest curvature radius of the wall mid-line, is assumed to remain constant during the collapse,
- the mid-surface is deformed without extension.

The collapse is characterized by large variations in A_i under small variations of p before the contact configuration, where the opposite edges of the wetted perimeter touch (Fig. 21). Besides, these huge changes in tube transverse configuration for slightly negative transmural pressure are observed in any compliant pipe, whether the wall is uniform and homogeneous or is a composite material of non-uniform geometry [18], *in vitro* as well as *in vivo* [19].

The contact reactions induce discontinuities in the first derivative at the point-contact pressure (subscript c) $\partial A_i/\partial p\Big|_{p_c}$ and the second one at the line-contact pressure (subscript ℓ) $\partial^2 A_i/\partial p^2\Big|_{p_\ell}$ [20]. Such discontinuities affect probably the mechanical behaviour of the fluid-tube couple. The discontinuity in the first derivative at p_c is exhibited by a break in the slope of the tube law.

Normalization The tube law is illustrated for the negative transmural pressure range in Fig. 21, using the dimensionless quantities $\tilde{p} = p/K$ and $\tilde{A}_i = A_i/A_{i_0}$. Fig. **??** demonstrates that the tube law is affected by the unstressed elliticity.

In the pressure range $\tilde{p} \leq \tilde{p}_\ell$, the similarity law can be used down to $\sim -30\ \tilde{p}_\ell$ that is when the tube shape remains self-similar with the twin-lobed characteristic configuration. The pressure-area relationship for $\tilde{p} \leq \tilde{p}_\ell$ is generally expressed by the following equation:

$$\tilde{p} = -\mathcal{B}(k_0, h_0)\tilde{A}_i^{-n(k_0,h_0)}, \tag{6}$$

where $\mathcal{B}(k_0, h_0) = -\tilde{p}_\ell/\tilde{A}_{i\ell}$ [21].

Different experimental techniques have been developed to validate the mechanical model and to measure the cross-sectional area during experiments. The optical technique monitors the pipe shape and computes the complete cross sectional area over the whole tube length (*e.g.* [22]). The luminal area is obtained from the external tube geometry assuming a constant wall thickness during the deformation. Ultrasound imaging have been used as the reference method [23]. This method, which necessitates a careful positionning of the probes, is also proposed to compute the bending stiffness and derived mechanical quantities.

Input geometrical and mechanical data must be measured prior any investigation, because either they affect the tube law, or they play a role in the flow regime. The tube law depends indeed strongly on both tube geometry and rheology in the unstressed state (subscript 0). The main geometrical factors

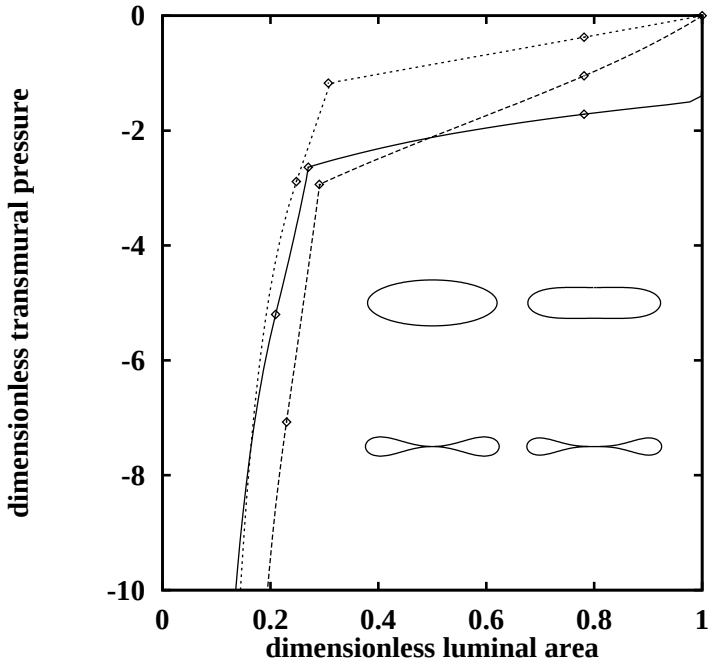

Figure 21: Numerical $\tilde{p}(\tilde{A}_i)$ laws for three ellipticities $k_0 = 1,005$ (continuous line), 2.8 (dashed line) and 10 (dotted line), with the characteristic values ($\diamond$) corresponding to the displayed characteristic shapes (unstressed elliptical, oval-shaped, point- and line-contact) (from [21]).

are (i) the tube ellipticity k_0 (k_0 is the ratio between the major semi axis a_0 and the minor semi axis of the neutral mid-line in the unstressed tube configuration) [20], and (ii) the wall thickness h_0 [21]. The bending stiffness K, used as the pressure scale, depends on the tube geometry and is proportional to the flexural rigidity $D = Eh_0^3/(12(1-\nu^2))$: $K = 2D/a_0^3$, where E and ν are the Young modulus and the Poisson coefficient respectively.

Whatever the investigation approach used, the tube law must be known in order to be able to interpret the experimental results or to develop a suitable computational model.

C Wave speed and critical flow rate

The speed c of propagation of small pressure wave in a long straight collapsible tube containing an incompressible fluid of mass density ρ is assumed to be given by the Moens-Korteweg equation:

$$c^2 = (A_i/\rho)(\partial p/\partial A_i) \tag{7}$$

The pressure wave of small amplitude, which propagates with the speed c, depends thus on the fluid inertia and the wall compliance (transverse propagation mode). This simple relationship is valid under the following additional assumptions : (i) purely elastic thin wall and constant geometry along the whole tube length of the reference configuration and negligible wall inertia, (ii) one-dimensional motion of the fluid.

The speed of the elasto-hydrodynamics coupling wave is computed from the tube law. Experimental observations have shown that the wave speed reaches its minimum when a contact between the opposite walls occurs [24]. In the slightly negative range of transmural pressures, both the tube cross-sectional area and the high compliance entail a low wave speed, associated to a high fluid velocity. Critical conditions (superscript $\star$) are reached when the local cross-sectional average fluid velocity $U(x)$ becomes equal to the wave speed c.

At each cross section can be associated a critical flow rate $q^\star$, which is related to the luminal area by $q^\star = A_i c$. Due to the discontinuity induced by the wall contact, the critical conditions must be different on the right ($q^\star_{c+}$) and on the left ($q^\star_{c-}$) side of the discontinuity (Fig 22, where the speed scale $(K/\rho)^{1/2}$ is used).

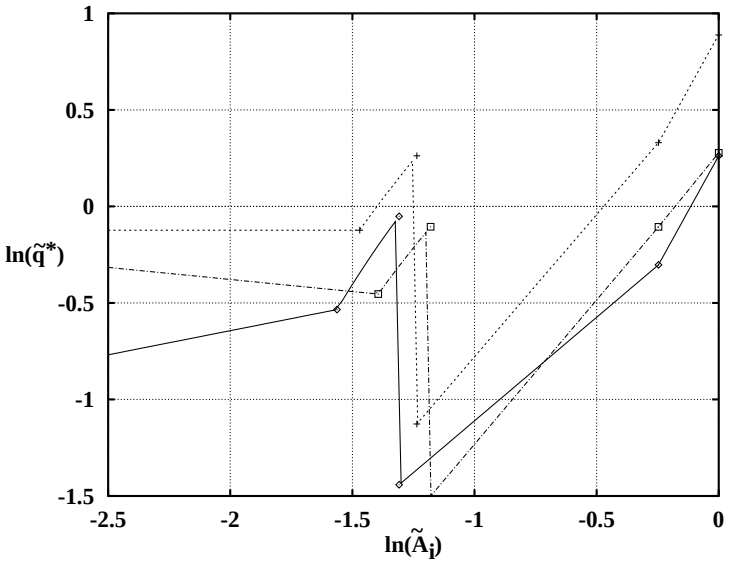

Figure 22: $\ln(\tilde{A}_i)$ *vs.* $\ln(\tilde{q}^\star)$ relationships for different tube ellipticities $k_0 = 1.005$ (continuous line), 2.8 (dotted line) and 10 (dashed line), with the characteristic values ($\tilde{A}_{i0}$, $\tilde{A}_{ip}$, $\tilde{A}_{ic}$, $\tilde{A}_{i\ell}$). When $p \leq p_\ell$, both the value and the sign of the slope of the relationship are affected by the tube ellipticity (from [21]).

References

[1] Shapiro A. H., Steady flow in collapsible tubes. ASME J. Biomech. Eng., 1977, 99, 126-147.

[2] Kamm R.D. and Pedley T.J., Flow in collapsible tubes: a brief review. ASME J. Biomech. Eng., 1989, 111, 177-179.

[3] Ribreau C., Thiriet M.,
Ecoulements veineux. In "Biomécanique", M.Y. Jaffrin & F. Goubel eds., Masson, Paris, 1998, p. 131-178.

[4] Thiriet M., Naili S., Langlet A., Ribreau C., Flow in thin-walled collapsible tubes. In "Biomechanics Systems Techniques and Applications", C. Leondes ed., Gordon & Breach, Newark, NJ, (in press).

[5] Ohba K., Sakurai A., Oka J., Self-excited oscillations in collapsible tube (laser-Doppler measurement of local flow field). Technol. Rep. Kansai Univ., 1989, 1-11.

[6] Bertram C.D. and Godbole S.A., LDA measurements of velocities in a simulated collapsed tube. ASME J. Biomech. Eng., 1997, 119, 357-363.

[7] Heil M. and Pedley T.J., Large post-buckling deformations of cylindrical shells conveying viscous flow. Journal of Fluids and Structures, 1996, 10, 565-599.

[8] Haond C., Ribreau C., Boutherin-Falson O. and Finet M., Laminar flow through collapsed veins. Morphometric response of endothelial vascular cells to a longitudinal shear stress non uniform cross-wise. European Physical Journal, Applied Physics (submitted).

[9] Ribreau C., Naili S., Bonis M., Langlet A. Collapse of thin-walled elliptical tubes for high values of major-to-minor axis ratio. ASME Journal of Biomechanical Engineering, 115, 1993, 432-440.

[10] Ribreau C., Merle D., Bonis M., Détermination expérimentale du module d'Young transversal d'une conduite élastique en dépression lors de son aplatissement. Conditions d'application aux veines. J. Biophysique Biomécanique, **10** (1986): 57-62.

[11] George P.L. et Borouchaki H., Delaunay triangulation and meshing. Applications to Finite Elements, Hermès, Paris, 1998.

[12] Conca C., Pares C., Pironneau O., Thiriet M., A computational model of Navier-Stokes equations with imposed pressure and velocity fluxes. Int. J. Numer. Methods in Fluids, 1995, 20, 267-287.

[13] Arnold D.N., Brezzi F., Fortin M., A stable finite element for the Stokes equation. Calcolo, 21, 1984, 337-344.

[14] Pironneau O., On the transport-diffusion algorithm and its application to the Navier-Stokes Equations. Numerische Mathematik, 38, 1982, 309-332.

[15] Glowinski R., Numerical methods for nonlinear variational problems, Springer Series in Computational Physics, Springer-Verlag, N.Y., 1984, 493 pp.

[16] Heil M., Stokes flow in collapsible tubes: computation and experiment. J. Fluid Mech., 1997, 353, 285-312.

[17] Luo X.Y. and Pedley T.J., A numerical simulation of unsteady flow in a two-dimensional collapsible channel. J. Fluid Mech., 1996, 314, 191-225.

[18] Begis D., Delpuech C., Le Tallec P., Loth L., Thiriet M., Vidrascu M., A finite element model of tracheal collapse. J. Appl. Physiol., 1988, 64, 1359-1368.

[19] Thiriet M., Maarek J.M., Chartrand D. A., Delpuech C., Davis L., Hatzfeld C., Chang H. K., Transverse images of the human thoracic trachea during forced expiration. J. Appl. Physiol., 1989, 67, 1032-1040.

[20] Bonis M., Ribreau C., Verchery G., Etude théorique et expérimentale de l'aplatissement d'un tube élastique en dépression. J. Meca. Appl., 1981, 5, 123-144.

[21] Ribreau C., Naili, S., Bonis, M., Langlet, A., Collapse of thin-walled elliptical tubes for high values of major-to-minor axis ratio. ASME J. Biomech. Eng., 1993, 115, 432-440.

[22] Thiriet M., Delpuech C., Piroird J.M., Magnin I., Banc de mesure optique de la déformation de conduites souples. Innov. Technol. Biol. Med., 1987, 8, 99-107.

[23] Ribreau C., Merle D., Bonis M., Détermination expérimentale du module d'Young transversal d'une conduite élastique en dépression lors de son aplatissement. Conditions d'application aux veines. J. Biophysique Biomécanique, 1986, 10, 57-62.

[24] Bonis M., Ribreau C., Wave speed in non circular collapsible ducts. ASME J. Biomech. Eng., 1981, 103, 27-31.

Unit de recherche INRIA Rocquencourt
Domaine de Voluceau - Rocquencourt - BP 105 - 78153 Le Chesnay Cedex (France)

Unit de recherche INRIA Lorraine : LORIA, Technople de Nancy-Brabois - Campus scientiøque
615, rue du Jardin Botanique - BP 101 - 54602 Villers-ls-Nancy Cedex (France)
Unit de recherche INRIA Rennes : IRISA, Campus universitaire de Beaulieu - 35042 Rennes Cedex (France)
Unit de recherche INRIA Rhne-Alpes : 655, avenue de l'Europe - 38330 Montbonnot-St-Martin (France)
Unit de recherche INRIA Sophia Antipolis : 2004, route des Lucioles - BP 93 - 06902 Sophia Antipolis Cedex (France)

diteur
INRIA - Domaine de Voluceau - Rocquencourt, BP 105 - 78153 Le Chesnay Cedex (France)
http://www.inria.fr
ISSN 0249-6399